Axial-Flux PM Machines With Variable Air Gap

Hendrik Vansompel, Peter Sergeant, Luc Dupré, and Alex Van den Bossche

***Abstract*—Laminated soft magnetic steel is very often used to manufacture the stator cores of axial-flux PM machines. However, as the magnetic flux typically has main components parallel to the lamination plane, different magnetic flux density levels may occur over the radial direction: High flux densities near the saturation level are found at the inner radius, while the laminations at the outer radius are used inefficiently. To obtain a leveled magnetic flux density, this paper introduces a radially varying air gap: At the inner radius, the air gap is increased, while at the outer radius, the air gap remains unchanged. This results in equal flux densities in the different lamination layers. As the total flux in the stator cores is decreased due to the variable air gap, the permanent-magnet thickness should be increased to compensate for this. The effect of a variable air gap is tested for both a low-grade non-oriented and a high-grade grain-oriented material. For both materials, the redistribution of the magnetic flux due to the variable air gap results in a significant decrease of the iron losses. In the presented prototype machine, the iron losses are reduced up to 8% by introducing a variable air gap. Finally, a prototype machine is constructed using an efficient manufacturing procedure to construct the laminated magnetic stator cores with variable air gap.**

***Index Terms*—Axial-flux machine, permanent-magnet generators, permanent magnets, variable air gap.**

I. Introduction

RECENTLY, axial-flux PM machine technology is emerging [1]–[5]: Axial-flux PM machines have high power density and excellent efficiency and are very often introduced for vehicle propulsion [6], [7] and small direct-drive wind-energy conversion systems [8]–[12].

Among the axial-flux PM machines, many topologies exist [13], [14]. The topology used in this paper is the double-rotor, single-stator, yokeless, and segmented-armature variant [15], [16]. As shown in Fig. 1, this topology has no stator yoke and the stator consists of individual stator cores. This modular stator construction allows easy manufacturing of the soft magnetic cores and facilitates the coil-winding process [17].

Manuscript received July 10, 2012; revised November 8, 2012 and January 3, 2013; accepted March 4, 2013. Date of publication March 18, 2013; date of current version August 9, 2013. This work was supported in part by the Research Fund of Ghent University (BOF-associatieonderzoeksproject 05V00609), in part by the Fund of Scientific Research Flanders (FWO) under Project G.0082.06 and Project G.0665.06, in part by GOA under Project BOF 07/GOA/006, and in part by IAP under Project P6/21.

H. Vansompel, L. Dupré, and A. Van den Bossche are with Ghent University, B-9000 Ghent, Belgium (e-mail: hendrik.vansompel@ugent.be; luc.dupre@ugent.be).

P. Sergeant is with the Department Electrotechnology, Faculty of Applied Engineering Sciences, University College Ghent, B-9000 Ghent, Belgium (e-mail: peter.sergeant@ugent.be).

Color versions of one or more of the figures in this paper are available online at http://ieeexplore.ieee.org.

Digital Object Identifier 10.1109/TIE.2013.2253068

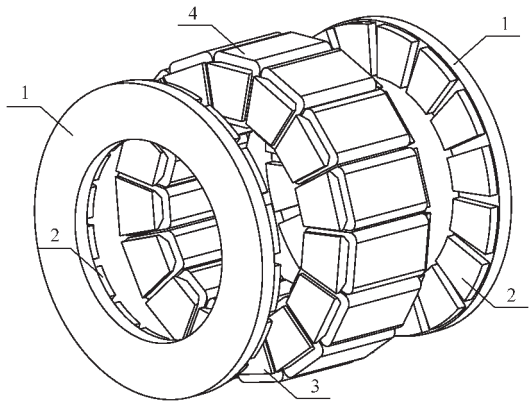

Fig. 1. Double-rotor, single-stator, yokeless, and segmented-armature axial-flux PM machine. (1) Rotor disk, (2) permanent magnet, (3) stator-core element, and (4) winding.

The individual core elements are made of laminated soft magnetic steel [18], [19], soft magnetic composites [20]–[22], or amorphous iron [23]. Among these different materials, amorphous iron is only rarely used because of its difficult machinability. Using soft magnetic composites, the 3-D geometry of the individual core can be easily obtained. Moreover, the magnetic properties of the material are isotropic, allowing complex 3-D magnetic flux paths in the core element. Despite the benefits of soft magnetic composites, the prototype machine discussed in this paper uses laminated soft magnetic steel. In comparison with the other proposed materials, laminated soft magnetic steel has lower cost and machining can be easily done. Moreover, [24] showed that using grain-oriented materials has a major impact on the reduction of stator-core loss.

However, whereas soft magnetic composites allow 3-D magnetic flux paths in the stator cores, in laminated soft magnetic steel, mainly magnetic fluxes parallel to the lamination plane exist. Only at the saturation level, magnetic fluxes migrate between adjacent laminations. As these magnetic fluxes are perpendicular to the lamination plane, additional losses due to eddy currents occur. The saturation of specific zones in the laminated magnetic cores should thus be avoided.

In Fig. 2, a cross-sectional view of the lamination at the inner and the outer radius of the axial-flux machine is presented. Both views are taken at the (same) angular position, when the magnetic flux in the stator-core element is at its maximum. As Fig. 2 shows, the magnetic flux density is much higher in the laminations at the inner radius than at the outer radius. This variation of the magnetic flux density over the radius is influenced by two parameters. First, the magnetic flux density corresponding to the permanent magnets is not constant over the radial direction for each rotor position. Leveling the flux over the radial direction can be obtained by varying the

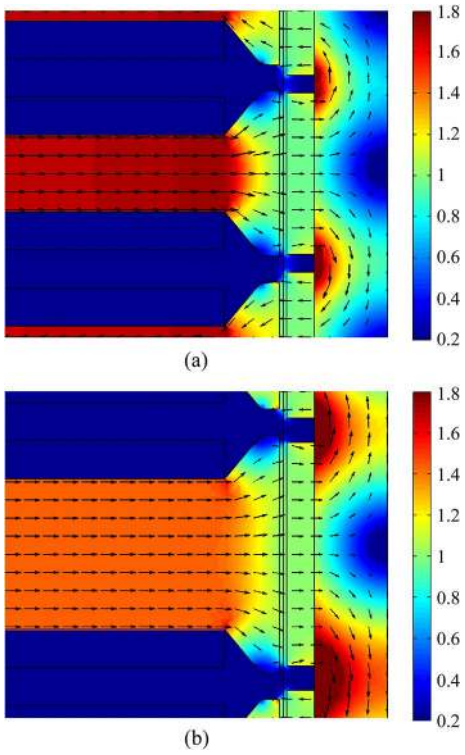

Fig. 2. Magnetic flux density distribution in the lamination when the magnetic flux in the lamination is maximal (a) for a lamination at the inner radius and (b) for a lamination at the outer radius with a constant air gap.

shape of the permanent magnets. However, the optimization of the permanent-magnet shape is commonly used for cogging torque minimization or mitigation of magnetic pull [25]–[29]. Therefore, leveling the flux density over the radial direction by reshaping the permanent magnets is not always possible. A second source of radially varying flux density levels is caused by the armature reaction. Stator currents result in an armature magnetic flux density that is higher at the laminations at the inner radius of the core than at the outer radius.

The addition of these two magnetic fluxes results in a magnetic flux density that strongly varies with the radial direction. Laminations at the outer radius are used inefficiently while saturation of the inner laminations may occur already. This unequal magnetic flux distribution will also have a major impact on the torque output and the losses in the stator cores. The saturation of the material at the inner side limits the torque output in this region, while the local high flux density values in these zones result in high core losses.

In this paper, a variable air gap is introduced, which allows us to obtain magnetic flux leveling in the radial direction. By making the air gap wider at the inner radius, the magnetic flux density is reduced, reaching the level of the laminations at the outer radius. As this variable air gap decreases the global flux density in the stator core, the permanent-magnet thickness is slightly increased to compensate for this. As will be shown later in this paper, introducing a variable air gap will have a positive impact on torque output and core losses.

In the following section, the variable air gap is discussed in more detail. In the subsequent section, the finite-element model used, including the material models, are presented. Subsequently, the effect of a variable air gap on the torque output and losses in the stator cores is examined. The final section focuses on an experimental prototype.

TABLE I
CHARACTERISTICS AND PARAMETERS OF THE AXIAL-FLUX PM MACHINE PROTOTYPE

Parameter	Value
Electrical output power (W)	4000
Rated speed (rpm)	2500
Rated torque (Nm)	15
Pole number	16
Slot/tooth number	15
Outer diameter (mm)	148
Inner diameter (mm)	100
Axial length (mm)	90
Active mass (kg)	8.5
Magnet width (mm)	0.8 τ_p
Magnets	NdFeB, 1.26T
Magnet thickness (mm)	2.5
Rotor backiron thickness (mm)	8
Airgap length (mm)	1
Slot width (mm)	12

The aim of this paper is to introduce the concept of a variable air gap and to point out the main benefits. Although these benefits are qualitatively valid to a wide range of axial-flux PM machines, the quantitative results are only mentioned for the existing prototype machine of which the main characteristics are listed in Table I.

II. VARIABLE AIR GAP

A. Flux Leveling Through Variable Air Gap

As mentioned already in Section I, Fig. 2 clearly shows that the laminations at the inner radius of the machine are already saturated while the laminations at the outer radius can carry more flux. The saturation of the laminations at the inner radius limits the torque output, while the lower magnetic flux densities in the laminations at the upper side result in inefficient torque production. Moreover, the local high flux density values at the inner radius will result in significantly high local core losses.

To overcome this issue, the magnetic flux densities at all radii should be brought to the same level. This can be realized in two different ways: one, by reducing the permanent-magnet thickness as a function of the radial position and keeping the original air gap unchanged or, two, by increasing the air gap width as a function of the radius while keeping the permanent-magnet thickness constant. As the first results in complex 3-D magnet shapes, the second method is implemented in this paper. With the manufacturing process presented in the last paragraph, the introduction of a variable air gap does not substantially diversify the machining.

Note that an increased air-gap width decreases the total flux through the stator-core element. Therefore, the permanent-magnet thickness should be increased to compensate for this.

To illustrate the concept of a variable air gap, a linear variable air gap is examined in this paper. In Fig. 3, a cross-sectional view of a segment of the axial-flux PM machine is depicted for a constant and linear variable air gap.

Fig. 4 illustrates the effect of a variable air gap on the magnetic flux density distribution. Starting from the original

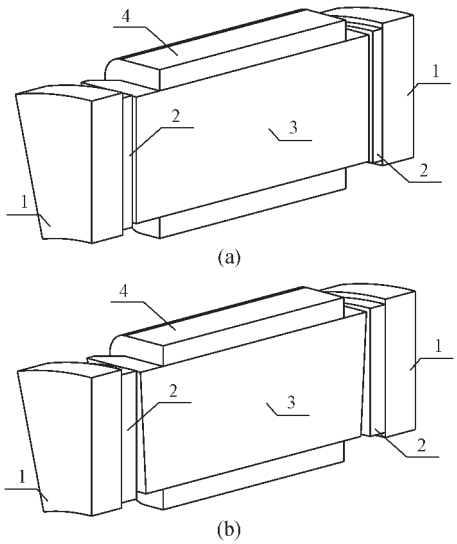

Fig. 3. Cross-sectional view of a segment of the axial-flux PM machine for (a) constant air gap and (b) variable air gap including (1) rotor disks, (2) permanent magnets, (3) stator-core element, and (4) winding.

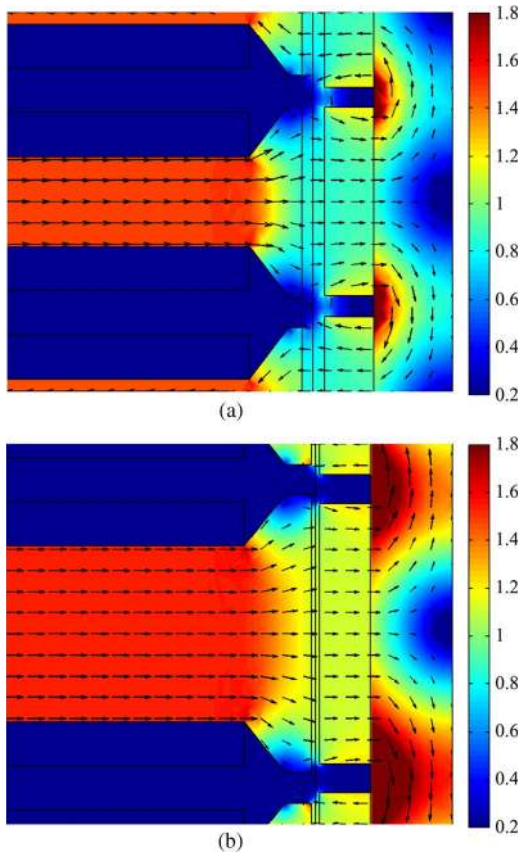

Fig. 4. Magnetic flux density distribution in the lamination when the magnetic flux in the lamination is maximal (a) for a lamination at the inner radius and (b) for a lamination at the outer radius with a radially linear variable air gap.

situation presented in Fig. 2, an additional linearly varying air gap is added to the existing 1-mm air gap in the original situation. This supplementary air gap ranges from 1.25 mm at the inner radius to 0 mm at the outer radius. In order to keep the total flux in the core constant, the permanent-magnet thickness is increased from 2.5 to 4 mm.

A comparison between the original situation, Fig. 2, and the new situation with variable air gap, Fig. 4, shows a uniform flux density over the radial direction. Due to the permanent-magnet thickness compensation, higher magnetic fluxes are found at the outer radius, while at the inner radius, the magnetic flux density is decreased below the saturation level.

B. Applicability of a Variable Air Gap

An important remark with respect to the variable air gap is the applicability. As illustrated in the previous section, a variable air gap is used when significant gradients in flux density levels over the different lamination layers occur. Several parameters do have an influence on this: the number of stator slots, stator slot-to-pole pair ratio, outer-to-inner diameter ratio, magnet shape, slot width, etc. For example, a small number of wide slots combined with a large outer-to-inner diameter ratio and rectangular magnets will result in a large flux density gradient over the laminations. In contrast, a large number of small slots combined with a small outer-to-inner diameter ratio and trapezoidal magnets will result in a more or less equal flux density in the laminations. The higher the gradient in flux density is, the higher the benefits of a variable air gap will be.

As it does not make sense to make a quantitative research of the many combinations, the benefits of a variable air gap are discussed qualitatively for the suggested prototype machine geometry. Only a choice of two soft magnetic materials, low-grade non-oriented and high-grade grain-oriented, is made to demonstrate that both materials benefit from a variable air gap.

III. Finite-Element Analysis

A. Multilayer 2-D Finite-Element Analysis

As laminated soft magnetic steel is used for the manufacturing of the core, magnetic fluxes parallel to the direction of the lamination plane are assumed. Therefore, the multilayer 2-D finite-element model [30], [31] illustrated in Fig. 5 is used. This modeling technique is very appropriate with respect to this research as it considers each lamination layer individually, not taking into account fluxes perpendicular to the lamination plane. After the simulation of the different 2-D finite-element models, the global quantities like torque output and core losses are retrieved by summation over the different 2-D model contributions.

B. Modeling Non-Oriented Material

Crucial in this research is the proper modeling of the soft magnetic material used in the stator cores. The nonlinear behavior of the stator-core material will influence the torque output, while the magnetic flux density pattern in the core laminations will determine the core losses.

The nonlinear characteristic of the material is modeled by specifying the $\mu_r(B)$ characteristic when solving the magnetic vector potential $\mathbf{A}$ equation

$$\nabla \times \left(\frac{1}{\mu_0 \mu_r(B)} \nabla \times \mathbf{A} \right) = \mathbf{J}_e \tag{1}$$

where $\mathbf{J}_e$ is the externally imposed current density.

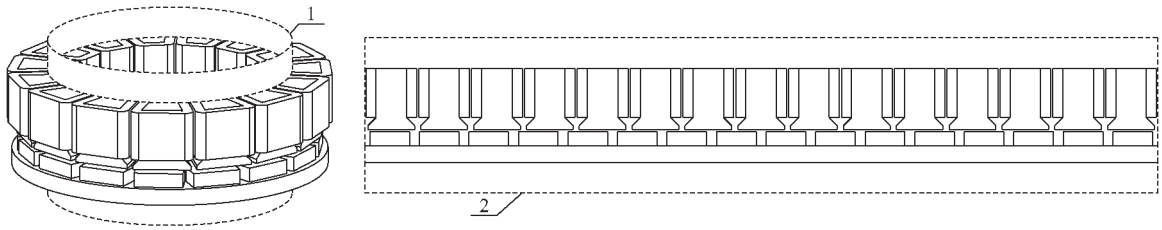

Fig. 5. Principle of the multilayer 2-D or quasi 3-D finite-element model: (1) Defining a cylindrical surface in the axial-flux PM machine and (2) subsequently unrolling this surface into a 2-D plane.

The calculation of the core losses is done *a posteriori* based on the simulated field waveforms. Therefore, B_x and B_y are determined in multiple points in the stator tooth.

The calculation of the core losses is separated into a hysteresis, a classical, and an excess loss component [32], [33]. While minor loops are absent, the hysteresis loss is determined by the peak value of the induction. Hysteresis losses are determined using a 1-D lookup table containing the hysteresis loss for several peak values.

The classical energy loss per cycle depends on the time derivative of $B(t)$

$$W_{\rm cl} = \frac{1}{12}\sigma d^2 \int_0^T \left(\frac{dB}{dt}\right)^2 {\rm d}t \tag{2}$$

where σ is the conductivity and d is the lamination thickness.

The instantaneous excess power loss $p_{\rm exc}(t)$ is given by

$$p_{\rm exc}(t) = \frac{n_o V_o}{2}\left(\sqrt{1+\frac{4\sigma GS}{n_o^2 V_o^2}\left|\frac{dB}{dt}\right|}-1\right)\left|\frac{dB}{dt}\right|. \tag{3}$$

In this equation, n_o is the number of simultaneously active magnetic objects for frequency $f \to 0$ and V_o defines the statistics of the magnetic objects. The dimensionless coefficient $G = 0.1356$ and the lamination cross section S are known constants.

The nonlinear characteristic $\mu_r(B)$ as well as the loss model coefficients are fitted from different measurements performed using an Epstein frame.

C. Modeling Grain-Oriented Material

The anisotropic-material and core-loss models used to model the grain-oriented data were adopted from [24]. The anisotropic-material model calculates the magnetization vector $\mathbf{M}$ as a function of the induction vector $\mathbf{B} = \nabla \times \mathbf{A}$. The equation for the magnetic potential $\mathbf{A}$ equals

$$\nabla \times \left(\frac{1}{\mu_0}\nabla \times \mathbf{A}\right) - \nabla \times \mathbf{M}(\nabla \times \mathbf{A}) = \mathbf{J}_e \tag{4}$$

where $\mathbf{J}_e$ is, again, the externally imposed current density.

As for the non-oriented material, the calculation of the core losses is done *a posteriori* based on the simulated field waveforms. By analyzing the simulated field waveforms, it is observed that no minor loops are present and that the field is only non-unidirectional in small parts of the tooth. However, in the small parts where the field is non-unidirectional, a dominant direction can be detected.

The same loss separation model as that for the non-oriented material is used. However, as the direction of the flux density pattern determines the losses, losses are quantified as the losses corresponding with a unidirectional waveform along the dominant direction. This waveform is obtained by projecting the $\mathbf{H}$-vector on the dominant direction.

The parameters that define the anisotropic-material and loss models are fitted from different measurements performed using an Epstein frame. Therefore, strips in seven different directions, 0°, 15°, 30°, 45°, 60°, 75°, and 90°, are cut from a sheet of grain-oriented material, and measurements are done with several frequencies and amplitudes for the magnetic field.

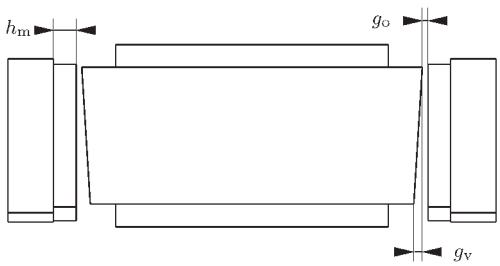

Fig. 6. Indication of the parameters that define a variable air gap on the cross section of a segment of the axial-flux PM machine with linear variable air gap: g_o is the original air gap width, g_v is the radial air gap variation, and h_m is the permanent-magnet thickness.

TABLE II
RANGES OF THE DOMAIN SCAN PARAMETERS

parameter	symbol	min [mm]	max [mm]
Permanent magnet thickness	$h_{\rm m}$	2.5	7.5
Radial airgap variation	$g_{\rm v}$	0	1.5

IV. TORQUE OUTPUT AND IRON LOSS COMPARISON

In Section II, it was illustrated that a variable air gap can result in an equal redistribution of the magnetic flux density over the radial direction. However, torque output and core losses were not discussed yet.

In this section, the influence of a variable air gap on the torque output and core losses is discussed. Therefore, a domain scan using two parameters is performed. These two parameters of interest are defined in Fig. 6, i.e., g_v is the value of the variable part of the air gap that is added to the original air gap g_o and h_m is the permanent-magnet thickness. The parameter ranges are summarized in Table II.

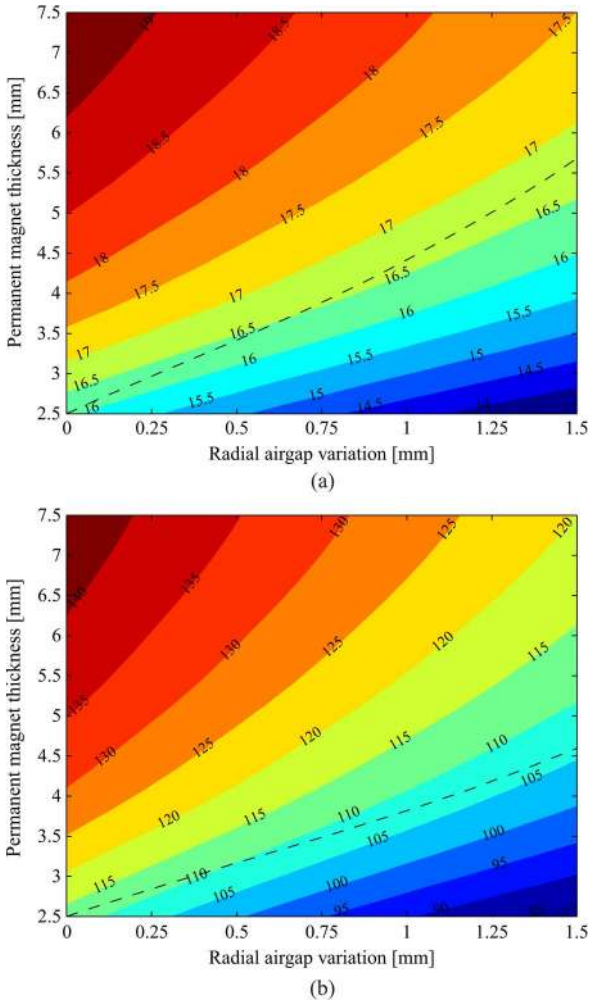

Fig. 7. (a) Torque output (in newton meters) and (b) core losses (in watts) as a function of radial air-gap variation g_v and permanent-magnet thickness h_m using the non-oriented material. The dashed lines indicate equicore losses and equitorque output, respectively.

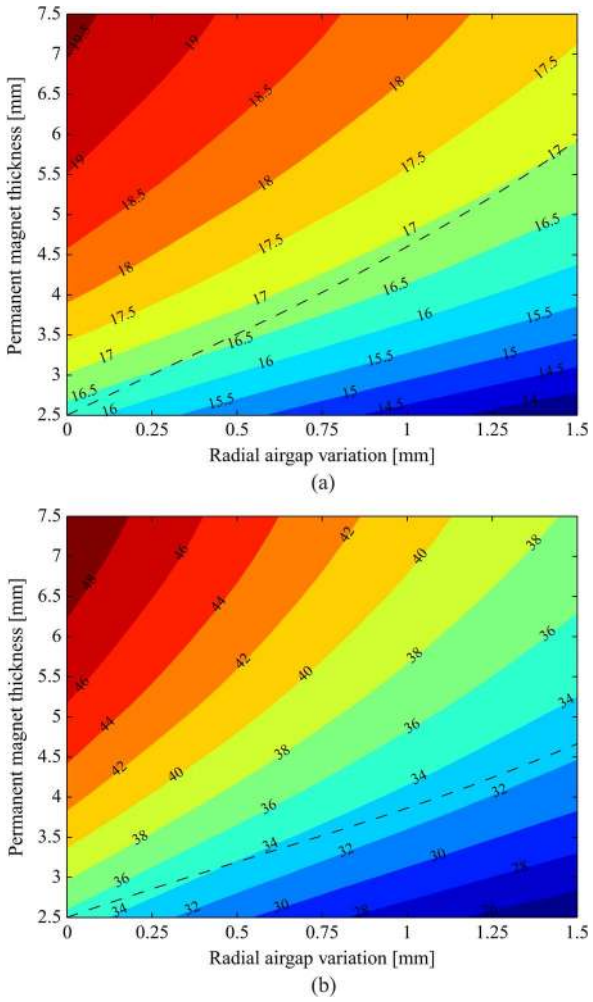

Fig. 8. (a) Torque output (in newton meters) and (b) core losses (in watts) as a function of radial air-gap variation g_v and permanent-magnet thickness h_m using the grain-oriented material. The dashed lines indicate equicore losses and equitorque output, respectively.

The simulations are performed with the multilayer 2-D finite-element model using six layers. The 15 stator coils are combined into a balanced three-phase system in which a sinusoidal current of 7 A is imposed. The phase of the current is chosen equal to the phase of the back-electromotive force. Therefore, the angular position at which the maximal flux density occurs (cf. Figs. 2 and 4) is slightly different from the position in which the magnet is aligned with the stator core. The non-oriented material is an M600-50A grade (6.0 W/kg at 1.5 T and 50 Hz), while the grain-oriented material has only 1.0 W/kg at 1.5 T and 50 Hz.

For each parameter set, the torque output and core losses are calculated and presented in Figs. 7 and 8 for the non- and grain-oriented materials, respectively. Notice that the point $g_v = 0$ mm and $h_m = 2.5$ mm corresponds to the original machine with constant air gap. For the grain-oriented material, the torque output is slightly higher, while much lower losses are found compared with the non-oriented material.

To compare the effect of a variable air gap for both material grades, two cases are studied in detail. In the first, the core losses are studied for a constant equal torque output. In the second case, the torque output is studied for a constant equal core loss. The reference values for the torque and core loss are set to these of the machine without a variable air gap, i.e., $g_v = 0$ and $h_m = 2.5$ mm.

On Figs. 7(a) and 8(a), the line of equal core loss is indicated in a dashed line. As the variable air gap increases, the dashed line indicates that this results in higher torque output. Similar results are found in Figs. 7(b) and 8(b), where lower core losses are found for the same output torque as the variable air gap increases. In both cases and for both materials, the introduction of a variable air gap is beneficial.

As mentioned before, the grain-oriented material has a slightly higher torque output, while significant lower losses are found compared with the non-oriented material. In Fig. 9, the relative torque increase and core-loss decrease as a function of the variable air gap are presented. The machine without a variable air gap, i.e., $g_v = 0$ and $h_m = 2.5$ mm, is chosen again as reference. For both cases, the high-grade grain-oriented material benefits the most from the variable air gap concerning the relative torque output and core loss. However, in terms of absolute values, the non-oriented material benefits the most. Note that increasing the torque output corresponds to a larger

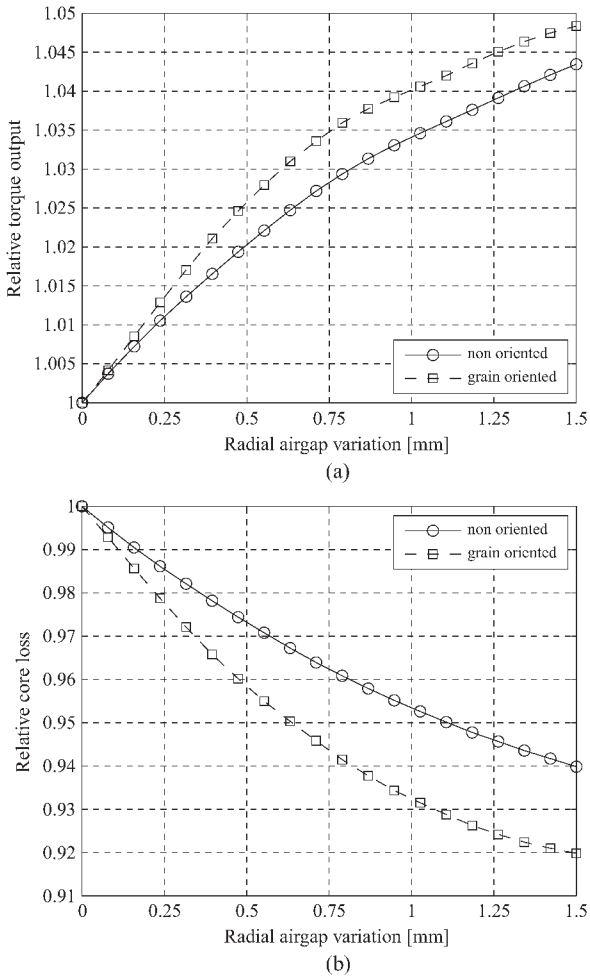

Fig. 9. Relative effect of a variable air gap on (a) the torque output for equicore losses and (b) the core losses for equitorque output for the non- and grain-oriented materials.

Fig. 10. Serpentine cut out of the soft magnetic material. The laminations are connected in the middle through little joints. Subsequently, the serpentine is folded into a stator-core element.

Fig. 11. Finished stator consisting of 15 premade stator-core elements. Axial positioning and fixation of the elements is achieved at the middle of the stator cores.

increase in permanent-magnet thickness than lowering the core losses for the same torque output.

As the aim of this work was to obtain an equal flux density distribution over the radial direction, proper values for the variable air gap and magnet height were selected by the investigation of the flux density distributions at different radii. A variable air gap of 0.9 mm and a magnet height of 3.5 mm were found to result in an equal distribution of the magnetic flux density over the radial direction. The cost of the additional 1-mm magnet height reduces the core losses by more than 4% for the same output power.

V. Experimental Verification

One important issue with respect to the variable air gap is the manufacturing of the stator cores out of the laminated electrical steel sheets. An obvious solution to obtain a variable air gap would be to take a stator core intended for a constant air gap and grind the excess material away. However, the grinding causes electrical contact between the lamination layers and thus increases the core losses.

The solution proposed in this paper is presented in Fig. 10. In the figure, a serpentine is cut out of a laminated electrical steel sheet. This serpentine consists of multiple laminations that are connected in the middle part through small joints. After the serpentine is cut, the joints act like hinges when the serpentine is folded into a finished stator coil. The enlarged portion in the middle part is used for the axial fixation of the cores during the assembly of the finished stator.

A winding is placed around each individual core. Then, the cores are assembled into the stator. This manufacturing process finally results in the finished stator, as shown in Fig. 11. This prototype machine is used for the experimental verification of the finite-element and anisotropic-material models in particular.

To perform measurements on the suggested prototype axial-flux PM machine, an experimental setup was built. In this setup, the axial-flux PM machine is connected to a two-pole 7.5-kW induction motor via a torque sensor. This induction motor is fed by an 11-kW inverter that is controlled by LabVIEW. An optical position sensor is used to obtain the shaft speed, and a voltage measurement on the terminals of the axial-flux PM machine is performed. Although each phase consists of five teeth, the winding of each individual tooth is accessible. The data retrieved from voltage, torque, and speed measurements are sampled by a National Instruments data-acquisition system with a sampling speed of up to 250 kSamples/s.

During the measurements at load, the prototype machine is used as a generator and connected to a 30-Ω resistance. The simulated and measured phase voltage and current waveforms

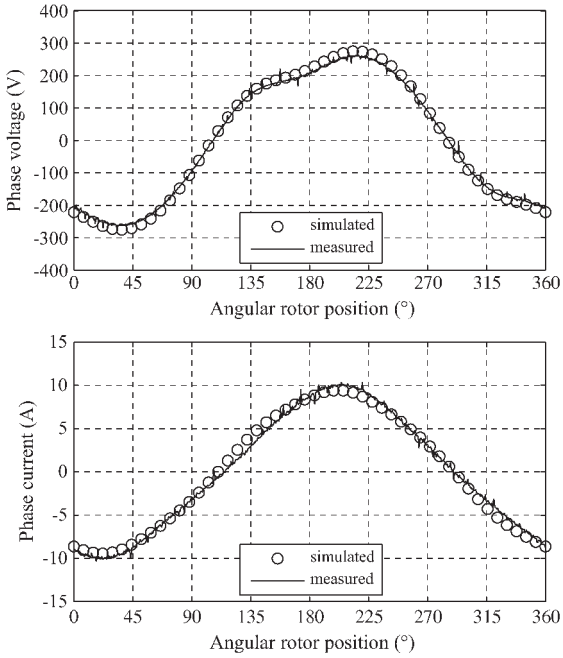

Fig. 12. Simulated and measured phase voltage and current waveforms at 2500 r/min.

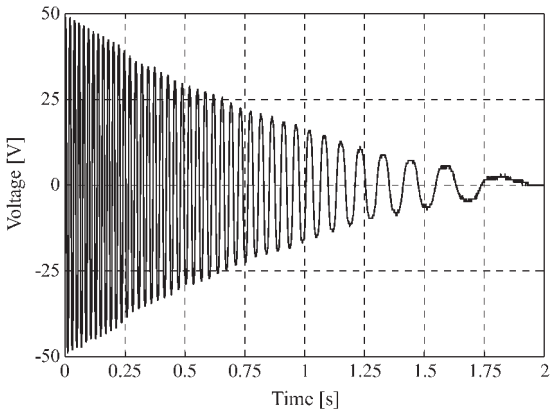

Fig. 13. Run-out test of the AFPMSM prototype machine at no load starting from 400 r/min.

are shown in Fig. 12. Good correspondence between both simulated and measured data is found.

At the nominal speed of 2500 r/min, an electrical power output of 4048 W was measured. By subtraction of the mechanical input measured via the torque sensor mounted on the axis and the electrical power output, an indication of the power losses is retrieved. Next to the core and iron losses, also eddy current losses in the permanent magnets, mechanical losses in the bearings, and windage losses are present. At the load conditions shown in Fig. 12, a power loss of 250 W is measured.

The losses at no load can be compared with the losses obtained from a run-out test: $J(d\Omega)/(dt) = -T_{\rm loss}$, with Ω as the mechanical speed and $T_{\rm loss}$ as the loss torque. The inertia J was estimated at $0.0107\ \mathrm{kg \cdot m^2}$. Fig. 13 shows a run-out test from 400 r/min. The recorded voltage makes it possible to determine at any moment the speed and its time derivative. From these data, the experimental total loss can be found as a function of the frequency. This total loss consists of the losses in the bearings, losses in the magnetic material in the stator cores [24], [34], [35], and eddy current losses in the permanent magnets and rotor [36]. A comparison revealed that the measured total loss (obtained through the run-out test) was higher than the simulated loss: 15 W compared with the 2.89 W in the stator cores. This difference is explained by the dominant bearing losses, significant eddy current losses [36] in the permanent magnets, and deterioration of the stator-core material by laser cutting.

VI. Conclusion

Laminated soft magnetic steel is very often used to manufacture the stator cores of axial-flux PM machines. Soft magnetic steel sheets have good machinability, and low iron losses are achievable when grain-oriented material is used. However, the magnetic flux density typically has main components parallel to the lamination plane. As a result, different magnetic flux density levels may occur over the radial direction: High flux densities near the saturation level are found at the inner radius, while the laminations at the outer radius are used inefficiently. To get an equal flux density distribution, this paper has introduced a variable air gap. At the inner radius, the air gap is increased, while at the outer radius, the air gap remains unchanged. As the total flux in the laminations is decreased due to the variable air gap, the permanent-magnet thickness is enlarged to compensate for this. The redistribution of the magnetic flux due to the variable air gap results in a significant decrease of the core losses. In the prototype machine, the core losses are reduced by 8% by introducing a variable air gap. Finally, an efficient manufacturing procedure is proposed to construct the stator cores with variable air gap.

References

[1] M. Aydin, S. Huang, and T. A. Lipo, "Design, analysis, and control of a hybrid field-controlled axial-flux permanent-magnet motor," *IEEE Trans. Ind. Electron.*, vol. 57, no. 1, pp. 78–87, Jan. 2010.

[2] Y. Kano, T. Kosaka, and N. Matsui, "A simple nonlinear magnetic analysis for axial-flux permanent-magnet machines," *IEEE Trans. Ind. Electron.*, vol. 57, no. 6, pp. 2124–2133, Jun. 2010.

[3] W. Fei, P. C. K. Luk, and T. S. El-Hasan, "Rotor integrity design for a high-speed modular air-cored axial-flux permanent-magnet generator," *IEEE Trans. Ind. Electron.*, vol. 58, no. 9, pp. 3848–3858, Sep. 2011.

[4] F. Caricchi, F. Maradei, G. De Donato, and F. G. Capponi, "Axial-flux permanent-magnet generator for induction heating gensets," *IEEE Trans. Ind. Electron.*, vol. 57, no. 1, pp. 128–137, Jan. 2010.

[5] G. De Donato, F. Giulii Capponi, and F. Caricchi, "On the use of magnetic wedges in axial flux permanent magnet machines," *IEEE Trans. Ind. Electron.*, vol. 60, no. 11, pp. 4831–4840, Nov. 2013.

[6] F. Crescimbini, A. Lidozzi, and L. Solero, "High-speed generator and multilevel converter for energy recovery in automotive systems," *IEEE Trans. Ind. Electron.*, vol. 59, no. 6, pp. 2678–2688, Jun. 2012.

[7] Y. P. Yang and D. S. Chuang, "Optimal design and control of a wheel motor for electric passenger cars," *IEEE Trans. Magn.*, vol. 43, no. 1, pp. 51–61, Jan. 2007.

[8] A. Di Gerlando, G. Foglia, M. F. Iacchetti, and R. Perini, "Axial flux PM machines with concentrated armature windings: Design analysis and test validation of wind energy generators," *IEEE Trans. Ind. Electron.*, vol. 58, no. 9, pp. 3795–3805, Sep. 2011.

[9] T. F. Chan and L. L. Lai, "An axial-flux permanent-magnet synchronous generator for a direct-coupled wind-turbine system," *IEEE Trans. Energy Convers.*, vol. 22, no. 1, pp. 86–94, Mar. 2007.

[10] M. Andriollo, M. De Bortoli, G. Martinelli, A. Morini, and A. Tortella, "Permanent magnet axial flux disc generator for small wind turbines," in *Proc. 18th Int. Conf. Elect. Mach.*, Sep. 6–9, 2008, pp. 1–6.

[11] T. F. Chan, L. L. Lai, and X. Shuming, "Field computation for an axial flux permanent-magnet synchronous generator," *IEEE Trans. Energy Convers.*, vol. 24, no. 1, pp. 1–11, Mar. 2009.
[12] T. F. Chan, W. Weimin, and L. L. Lai, "Performance of an axial-flux permanent magnet synchronous generator from 3-D finite-element analysis," *IEEE Trans. Energy Convers.*, vol. 25, no. 3, pp. 669–676, Sep. 2010.
[13] T. D. Nguyen, K.-J. Tseng, S. Zhang, and H. T. Nguyen, "A novel axial flux permanent-magnet machine for flywheel energy storage system: Design and analysis," *IEEE Trans. Ind. Electron.*, vol. 58, no. 9, pp. 3784–3794, Sep. 2011.
[14] M. Aydin, S. Huang, and T. A. Lipo, "Torque quality and comparison of internal and external rotor axial flux surface-magnet disc machines," *IEEE Trans. Ind. Electron.*, vol. 53, no. 3, pp. 822–830, Jun. 2006.
[15] T. J. Woolmer and M. D. McCulloch, "Analysis of the yokeless and segmented armature machine," in *Proc. IEEE Int. Elect. Mach. Drives Conf.*, pp. 704–708, May 3–5, 2007.
[16] W. Fei and P. C. K. Luk, "Cogging torque reduction techniques for axial-flux surface-mounted permanent-magnet segmented-armature-torus machines," in *Proc. IEEE Int. Symp. Ind. Electron.*, Jun. 30/Jul. 2, 2008, pp. 485–490.
[17] W. Fei, P. Luk, and K. Jinupun, "A new axial flux permanent magnet segmented-armature-torus machine for in-wheel direct drive applications," in *Proc. IEEE Power Electron. Spec. Conf.*, Jun. 15–19, 2008, pp. 2197–2202.
[18] G. De Donato, F. G. Capponi, and F. Caricchi, "No-load performance of axial flux permanent magnet machines mounting magnetic wedges," *IEEE Trans. Ind. Electron.*, vol. 59, no. 10, pp. 3768–3779, Oct. 2012.
[19] A. B. Letelier, D. A. Conzalez, J. A. Tapia, R. Wallace, and M. A. Valenzuela, "Cogging torque reduction in an axial flux PM machine via stator slot displacement and skewing," *IEEE Trans. Ind. Appl.*, vol. 43, no. 3, pp. 685–693, May/Jun. 2007.
[20] R. Di Stefano and F. Marignetti, "Electromagnetic analysis of axial-flux permanent magnet synchronous machines with fractional windings with experimental validation," *IEEE Trans. Ind. Electron.*, vol. 59, no. 6, pp. 2573–2582, Jun. 2012.
[21] G. S. Liew, N. Ertugrul, W. L. Soong, and D. B. Gehlert, "Analysis and performance evaluation of an axial-field brushless PM machine utilising soft magnetic composites," in *Proc. IEEE Int. Elect. Mach. Drives Conf.*, May 2007, pp. 153–158.
[22] S. M. A. Sharkh and M. T. N. Mohammad, "Axial field permanent magnet DC motor with powder iron armature," *IEEE Trans. Energy Convers.*, vol. 22, no. 3, pp. 608–613, Sep. 2007.
[23] Z. Wang, Y. Enomoto, M. Ito, R. Masaki, S. Morinaga, H. Itabashi, and S. Tanigawa, "New permanent magnet synchronous motors with amorphous rolled cores," in *Book Abstr. Soft Magn. Mater. Conf.*, Sep. 2011, p. A2-08.
[24] D. Kowal, P. Sergeant, L. Dupré, and A. Van den Bossche, "Comparison of non-oriented material and grain oriented material for an axial flux permanent-magnet machine," *IEEE Trans. Magn.*, vol. 46, no. 2, pp. 279–285, Feb. 2010.
[25] J. H. Choi, J. H. Kim, D. H. Kim, and Y. S. Baek, "Design and parametric analysis of axial flux PM motors with minimized cogging torque," *IEEE Trans. Magn.*, vol. 45, no. 6, pp. 2855–2858, Jun. 2009.
[26] C.-C. Hwang, P.-L. Li, F. C. Chuang, C.-T. Liu, and K.-H. Huang, "Optimization for reduction of torque ripple in an axial flux permanent magnet machine," *IEEE Trans. Magn.*, vol. 45, no. 3, pp. 1760–1763, Mar. 2009.
[27] F. Caricchi, F. G. Capponi, F. Crescimbini, and L. Solero, "Experimental study on reducing cogging torque and no-load power loss in axial-flux permanent-magnet machines with slotted winding," *IEEE Trans. Ind. Appl.*, vol. 40, no. 4, pp. 1066–1075, Jul./Aug. 2004.
[28] G. Barakat, T. El-meslouhi, and B. Dakyo, "Analysis of the cogging torque behavior of a two-phase axial flux permanent magnet synchronous machine," *IEEE Trans. Magn.*, vol. 37, no. 4, pp. 2803–2805, Jul. 2001.
[29] D. A. Gonzalez, J. A. Tapia, and A. L. Bettancourt, "Design consideration to reduce cogging torque in axial flux permanent-magnet machines," *IEEE Trans. Magn.*, vol. 43, no. 8, pp. 3435–3440, Aug. 2007.
[30] R. J. Wang and M. J. Kamper, "Evaluation of Eddy current losses in axial flux permanent magnet (AFPM) machine with an ironless stator," in *Conf. Rec. 37th IEEE IAS Annu. Meeting*, Pittsburgh, PA, USA, Oct. 2002, pp. 1289–1294.
[31] A. Parviainen, M. Niemelä, and J. Pyrhänen, "Modeling of axial permanent-magnet machines," *IEEE Trans. Ind. Appl.*, vol. 40, no. 5, pp. 1333–1340, Sep./Oct. 2004.
[32] G. Bertotti, *Hysteresis in Magnetism*. New York, NY, USA: Academic, 1994, p. 401.
[33] E. Barbisio, F. Fiorillo, and C. Ragusa, "Predicting loss in magnetic steels under arbitrary induction waveform and with minor hysteresis loops," *IEEE Trans. Magn.*, vol. 40, no. 4, pp. 1810–1819, Jul. 2004.
[34] H. Vansompel, P. Sergeant, and L. Dupré, "Optimized design considering the mass influence of an axial flux permanent-magnet synchronous generator with concentrated pole windings," *IEEE Trans. Magn.*, vol. 46, no. 12, pp. 4101–4107, Dec. 2010.
[35] H. Vansompel, P. Sergeant, L. Dupré, and A. Van den Bossche, "Evaluation of a simple lamination stacking method for the teeth of an axial flux permanent-magnet synchronous machine with concentrated stator windings," *IEEE Trans. Magn.*, vol. 48, no. 2, pp. 999–1002, Feb. 2012.
[36] H. Vansompel, P. Sergeant, and L. Dupré, "A multilayer 2-D–2-D coupled model for eddy current calculation in the rotor of an axial-flux PM machine," *IEEE Trans. Energy Convers.*, vol. 27, no. 3, pp. 784–791, Sep. 2012.

Hendrik Vansompel was born in Belgium in 1986. He received the B.S. and M.S. degrees in electromechanical engineering from Ghent University, Ghent, Belgium, in 2008 and 2009, respectively, where he is currently working toward the Ph.D. degree at the Department of Electrical Energy, Systems and Automation.

His present research interests include electrical machine modeling and design, particularly for sustainable energy systems.

Peter Sergeant received the M.S. and Ph.D. degrees in electromechanical engineering from Ghent University, Ghent, Belgium, in 2001 and 2006, respectively.

He has been a Postdoctoral Researcher for the Fund of Scientific Research Flanders since 2006 and a Researcher with University College Ghent, Ghent, since 2008. His current research interests include numerical methods in combination with optimization techniques to design nonlinear electromagnetic systems, particularly electromagnetic actuators.

Luc Dupré was born in 1966. He received the Graduate degree in electrical and mechanical engineering and the Doctorate degree in applied sciences from Ghent University, Ghent, Belgium, in 1989 and 1995, respectively.

He is currently a Full Professor with the Faculty of Engineering and Architecture, Ghent University. His research interests mainly include numerical methods for electromagnetics, modeling, and characterization of soft magnetic materials, micromagnetism, inverse problems, and optimization in (bio)electromagnetism.

Alex Van den Bossche received the M.S. and Ph.D. degrees in electromechanical engineering from Ghent University, Ghent, Belgium, in 1980 and 1990, respectively.

He is with the Electrical Energy Laboratory, Ghent University, where he has been a Professor since 1993. His research is in the field of electrical drives, power electronics on various converter types, and passive components and magnetic materials. He is also interested in renewable energy conversion. He is an author of the book *Inductors and Transformers for Power Electronics* (CRC Press, 2005). He was a starter of the spin-off companies Inverto n.v. (1990) and, recently, Alenco n.v. (2009).